THE JOURNAL OF PHYSICAL CHEMISTRY Letters

pubs.acs.org/JPCL Letter

Reorganization of Interfacial Water by an Amphiphilic Cationic Surfactant Promotes CO_2 Reduction

Zhuo-Qun Zhang, Soumyodip Banerjee, V. Sara Thoi, and Anthony Shoji Hall*

Cite This: *J. Phys. Chem. Lett.* 2020, 11, 5457−5463 Read Online

ACCESS | Metrics & More | Article Recommendations | Supporting Information

ABSTRACT: The presence of cetyltrimethylammonium bromide (CTAB) near the surface of a Cu electrode promotes the electrochemical reduction of CO_2 to fuels. CTAB increases the CO_2 reduction rate by as much as 10× and decreased the HER rate by 4×, leading to ∼75% selectivity toward the reduction of CO_2. Surface enhanced infrared absorption spectroscopy (SEIRAS) was used to probe the effects of CTAB adsorption on the structure of interfacial water and CO_2 reduction intermediates. HER suppression was found to arise from the displacement of interfacial water molecules from CTAB adsorption within the double layer. The enhanced CO_2 reduction rate can be correlated to an increased population of atop-bound CO and the emergence of a low frequency atop-CO band. These results unravel the role of additives in improving CO_2-to-fuels electrocatalysis and establishing this as a powerful methodology for directing product selectivity.

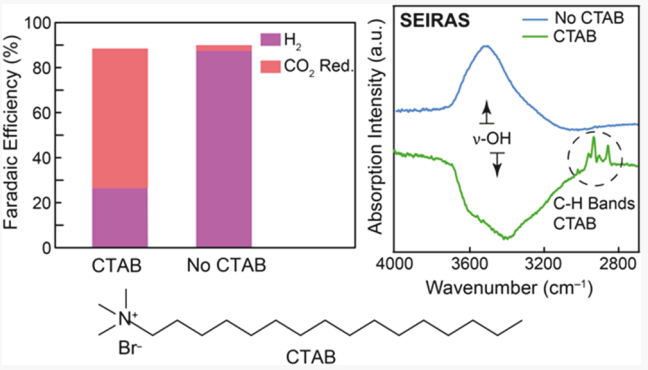

The electrocatalytic CO_2 reduction reaction (CO_2RR) is a promising method for producing high energy density fuels from intermittent renewable energy.[1−4] The CO_2RR requires high overpotentials to reach appreciable current densities, and suffers from poor product selectivity. Cu is one of the most promising electrode materials for reducing CO_2 to CO, $HCOO^-$, C_2H_4, CH_4, and higher order hydrocarbons at substantial rates.[3,5−8] However, the reduction of CO_2 must compete with the hydrogen evolution reaction (HER), eroding the CO_2RR efficiency.[9,10] It is important to design routes to inhibit HER, while allowing CO_2RR to proceed with high current efficiencies.

Understanding how to control the bifurcation between HER and CO_2RR is paramount for improving the current efficiency toward CO_2RR. One way to accomplish this is to regulate the liquid side of the catalyst interface by choosing the appropriate electrolyte conditions. Recently, the identity of cations in the electrolyte has been shown to impact the rate of CO_2RR and/or the HER rate.[11−15] For example, the rate of $HCOO^-$, C_2H_4, and CH_3OH production were found to increase by >∼10×, while the HER rate was invariant by changing the alkali metal cation from Li^+ to Cs^+.[12,14] Larger cations such as Cs^+ have been thought to promote CO_2RR by increasing the CO_2 concentration at the electrode surface and/or by stabilization of reaction intermediates from increased cation accumulation.[7,11,12,14,16] Recent studies have shown that molecular adsorbates can also improve the performance of various electrode materials for CO_2RR. For example, surface modification of electrodes by polymeric films prepared by electropolymerized pyridinium molecules, N-heterocylic carbenes, and the addition of molecular additives into the electrolyte, such as amphiphilic surfactants, ionic liquids, *n*-alkylammonium salts, and pyridine, have been found to improve CO_2RR.[13,17−24] The molecular promotors for these systems have, in most cases, been observed to promote the rate of CO_2RR while simultaneously suppressing HER. Density functional theory (DFT) has been invaluable in explaining how the adsorption of various molecular species impacts CO_2RR catalysis. However, little to no explanation is given to explain the suppression of the competing HER reaction.

Understanding the role of HER suppression is critical for obtaining a clear picture of CO_2RR in aqueous electrolytes, but this has been hardly examined. One common theme among the molecular promotors mentioned above is that most of the molecules are hydrophobic in nature. We hypothesize that the adsorption of such species can perturb the interfacial water structure, influencing the rate of HER. To the best of our knowledge, there is only one report that probes the influence of the interfacial water structure during a reaction related to CO_2RR. Waegele et. al utilized SEIRAS to show that isolated

Received: May 1, 2020
Accepted: June 11, 2020
Published: June 11, 2020

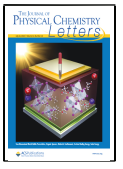

water species were removed from the interface by the adsorption of tetraalkylammonium ions, inhibiting the formation of ethylene from the reduction of CO.[25] However, no information regarding the HER suppression was provided in this report, and no such report exists for CO_2RR. Although interesting knowledge regarding water structure effects in electrocatalysis was provided, it does not answer the central question of how surface adsorbates control HER.

It is hypothesized that H_2O is the dominant proton donor in CO_2RR and the HER reaction, as evidenced by our earlier work on porosity-dependent CO_2 electrocatalysis, which shows a strong dependence on porosity, and by Wang et al., who have shown that the concentration of H_2O in water-in-salt electrolytes directly impacts the rate of CO_2RR and HER.[9,26,27] Furthermore, a recent report by Koper et al. has shown that the rate of CO_2RR and HER on group 11 metals exhibits a dependence on the electrode rotation rate in Ar- and CO_2-saturated 0.1 M $NaHCO_3$, hinting that H_2O is a facile proton donor under these reaction conditions.[28,29] If we are to fully understand how molecular additives promote CO_2RR and suppress HER, we need to systematically understand how the adsorption of species affects the dynamics of the interfacial water structure.

Cetyltrimethylammonium bromide (CTAB) is a particularly interesting molecular promotor, because it is cheap and commercially available in large quantities. Our recent report indicated that CTAB promoted the performance of CO_2RR and suppressed HER on Cu electrodes; a reduction of the double-layer capacitance indicated that CTAB was present within the double layer.[13] We also found that CTAB adsorption onto a nitrile modified electrode can produce large interfacial electric fields up to −1.25 V/nm, as probed by vibrational Stark shift spectroscopy under noncatalytic conditions.[13,23,24,30] Taken together, we hypothesized that the hydrophobic backbone of CTAB modified the concentration of interfacial water and that large interfacial electric fields suppressed the HER rate and the enhanced CO_2RR rate, respectively.

Herein, we provide a SEIRAS study of the CO_2RR with CTAB as a molecular promotor, unravelling its role for suppressing HER and enhancing the CO_2RR on Cu electrodes. The SEIRA effect enhances the sensitivity of adsorbates present within the first several monolayers of the electrode surface, which makes it ideal for probing species within the double layer.[31−33] We reveal that CTAB accumulation and reorganization near the electrode interface disrupt the hydrogen-bonding structure of water, decreasing its interfacial concentration. A reduction in the interfacial concentration of H_2O, the principal proton donor, was systematically correlated to the suppression of HER. Additionally, the presence of CTAB can modify the distribution and potential-dependence of specifically adsorbed CO, leading to increases in the rate of CO_2RR. This study provides insights into how molecular adsorbates modify the dynamics of interfacial H_2O and CO_2RR-related intermediates, shedding light on the delicate nature of adsorbates and their role in controlling interfacial catalysis.

We probed the CO_2RR on Cu electrodes in 0.1 M $NaHCO_3$ electrolytes (pH 6.8) purified with Chelex to remove trace metal contamination and used a leakless Ag/AgCl reference electrode (eDAQ).[34,35] In the electrochemical reduction of CO_2 on Cu foils, the addition of CTAB to the electrolyte led to a suppression of the HER Faradaic efficiency (FE) by ∼30 to 60% depending on the voltage (E) and to an enhancement in the CO_2RR FE by ∼40 to 60% (Figure S1a,b). A suppression of the HER current density for E more negative than −0.5 V vs the reversible hydrogen electrode (RHE, henceforth all voltages will be referenced to RHE unless otherwise noted) and an enhancement of the CO_2RR current density at all voltages decreased the FE for HER and improved the FE for CO_2RR (Figure S1). The primary product for CO_2RR was 50 to 60% $HCOO^-$ and ≤10% CO for the CTAB-containing electrolytes at all voltages (Figure S2). In CTAB-free electrolytes, mostly HER was observed until −1.0 V, where ∼15% FE for hydrocarbon products (CH_4 and C_2H_4) was observed (Figure S2). The Faradaic efficiency and partial current densities for the CO_2RR on the Cu foil control samples measured in the absence of CTAB are comparable to samples collected in $NaHCO_3$ electrolytes in other reports.[12,14] These results are consistent with our hypothesis that local CTAB accumulation modulates the electrode−electrolyte interface and affects the product selectivity.

SEIRAS measurements were collected on face-angled Cu-coated Si prisms under in CO_2-saturated electrolytes to interrogate the potential-dependence of species near the electrode surface during the CO_2RR(Figures S3 and S4). The CO_2RR performance of the Cu-coated Si prisms exhibited similar trends to those on Cu foil (Figures S1 and S5). The IR data was collected with ∼10 s resolution per spectrum and measured simultaneously by sweeping the voltage between 0.2 to −1.0 V at a 10 mV/s scan rate (Figures 1 and S6). Reference spectra for the SEIRAS measurements were recorded at 0.2 V in CO_2-saturated 0.1 M $NaHCO_3$ electrolyte

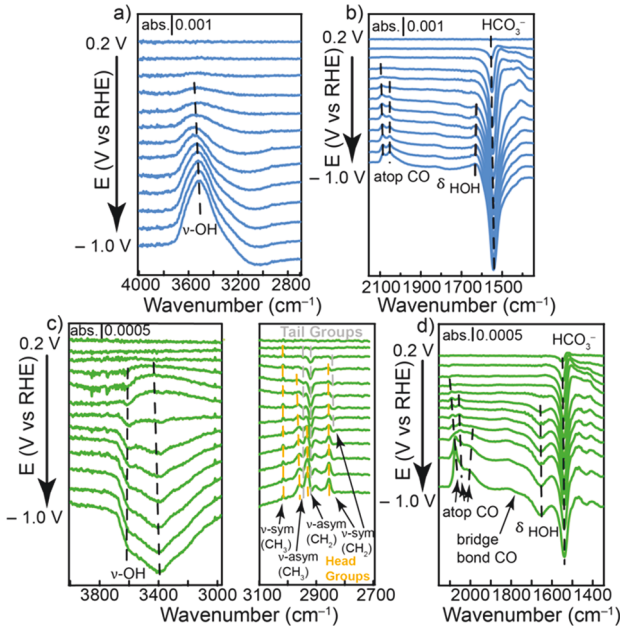

Figure 1. Representative infrared spectra of (a) ν-OH vibrational region of H_2O and (b) CO, δ_{HOH}, and OCO vibration of (bi)carbonate in CO_2-saturated 0.1 M $NaHCO_3$; (c) ν-OH vibrational region of H_2O and C−H vibrational bands of CTAB, gray and orange vertical lines denote the C−H groups of CTAB's head and tail, respectively; (d) CO, δ_{HOH}, and OCO vibration of (bi)carbonate in CO_2-saturated 0.1 M $NaHCO_3$ + 67 μM CTAB. All data was collected during a linear sweep voltammogram at a 10 mV s^{-1} scan rate, and the background spectrum was collected at 0.2 V vs RHE in the respective solutions.

https://dx.doi.org/10.1021/acs.jpclett.0c01334
J. Phys. Chem. Lett. 2020, 11, 5457−5463

with or without CTAB; the final spectra presented were subtracted from the reference spectrum collected in the same electrolyte, unless otherwise noted. We observed several vibrational bands between 3800 to 2800 cm^{-1}, which contain modes for interfacial water and the C−H bonds of CTAB, and between 2150 to 1400 cm^{-1}, which contain modes for adsorbed CO species, interfacial water, and interfacial (bi)carbonate (Figure 1 and S7).[22,36−41] The bands which point upward and downward indicate absorption and desorption of the band, respectively.

The roles of interfacial water and bicarbonate were probed with SEIRAS during a forward voltage sweep, from 0.2 to −1.0 V, in 0.1 M $NaHCO_3$ with and without 67 μM CTAB. Several vibrational bands were found to appear in at ∼3500, ∼1633, and ∼1550 cm^{-1}, which can be assigned to the O−H stretching mode (ν-OH) and HOH bending mode (δ_{HOH}) of water and the ν-OCO stretching mode of bicarbonate, respectively (Figure 1a,b).[36,38,39,41] The ν-OH and δ_{HOH} vibrational modes increased in intensity, and the bicarbonate band decreased in intensity during the forward E sweep. Based on previous SEIRAS studies, interfacial water molecules can change orientation in response to the voltage by reorienting to oxygen-up or oxygen-down configurations, which can be accompanied by a shift of the vibrational frequency of ν-OH from ∼3600 cm^{-1} (weakly hydrogen bonded) to ∼3200 cm^{-1} (strongly hydrogen bonded).[36,37,41,38,39] A sum frequency generation (SFG) study has suggested that that vibrational coupling can occur in the ν-OH region, obscuring information regarding the H-bonding structure.[42] However, this study was performed under conditions in which there were no external perturbations, only providing information for thermodynamically stable structures. Nevertheless, it is well accepted that potential difference spectra from SEIRAS can suggest that the increased intensity of interfacial ν-OH and δ_{HOH} bands with increasing negative voltage occurs from the reorienting of water with the protons tilted toward the electrode, aligning the dipole antiparallel toward the increasing negative surface charge, and/or by an increase in interfacial concentration from an electrowetting effect (Figure 1d).[38,43]

Cu electrodes were examined in CTAB-containing electrolytes under CO_2RR conditions to interrogate their effect on the dynamics of surface adsorbates (Figure 1c-d). Desorption bands for ν-OH, δ_{HOH}, and ν-OCO were observed when CTAB was added into the electrolyte at 0.2 V (open circuit potential), indicating that these species were displaced by CTAB at open circuit (Figure S8). This observation is consistent with the fact that CTAB is weakly solvated by water compared to Na^+ and likely forms weak ion pairs with (bi)carbonate and Br^-, allowing it to easily liberate its solvation shell and counterion to displace Na^+ from the interface. An increase in intensity of the ν-OH band, centered at ∼3450 cm^{-1}, was observed between −0.1 to −0.3 V; this observation is similar to what we observed in CTAB-free electrolytes (Figure 1a). However, as the voltage was swept more negative of −0.3 V, a bleach of the ν-OH band centered at ∼3600 cm^{-1} was observed, indicating the desorption of non-hydrogen-bonded (isolated) water molecules.[38,39] For voltages more negative than −0.5 V, a broad desorption band centered near ∼3400 cm^{-1} appeared and grew as the voltage was swept more negatively, showing that weakly hydrogen-bonded water was desorbing from the interface.[38,39] Similar to CTAB-free electrolytes, we observed desorption bands that correspond to (bi)carbonate as the voltage was swept negatively. We also collected SEIRAS spectra in electrolytes containing 67 μM NaBr + 0.1 M $NaHCO_3$ to isolate the role of Br^-; we found no significant differences of the ν-OH band and CO bands when compared to spectra collected in 0.1 M $NaHCO_3$ (Figure S9). The growth in intensity of the ν-OH desorption band at more negative voltages indicates that the structure of interfacial water is disrupted by the presence of CTAB, which is hydrophobic in nature.

To isolate the interfacial structure of CTAB and its influence on the water structure, we tracked changes in the CTAB adsorption bands as a function of potential (Figure 1c, right panel). Adsorption bands for several C−H stretching modes of CTAB appeared on the tail of the broad water band. These bands were centered at 3016 and 2959 cm^{-1}, which can be assigned to the symmetric and asymmetric C−H vibrational bands of the headgroup ($N-CH_3$), and the bands at 2931 and 2855 cm^{-1} could be assigned to the asymmetric C−H stretching mode and symmetric C−H stretching mode of CH_2 near the headgroup of CTAB.[44,45] The desorption bands centered at 2921 and 2846 cm^{-1} can be assigned to asymmetric and symmetric C−H stretching modes of CH_2 near CTAB's tail, respectively.[44,45] The bands for the headgroup increased in intensity as the voltage was swept more negatively, which indicated an increase in the interfacial concentrations of the headgroup, while we observe desorption bands from the CH_2 groups. These changes in intensity indicated that CTAB reoriented with its head pointing toward the electrode and increased in concentration as the voltage was swept negatively (Scheme 1).

Scheme 1. Potential-Dependent CTAB Adsorption and Reorientation in the Cathodic Scan and Its Impact on Interfacial Water Concentration under CO_2 Reduction Conditions[a]

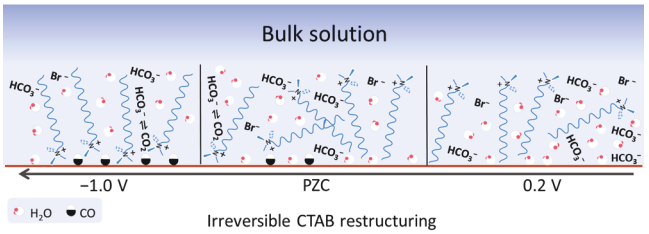

[a]The reorientation of CTAB is irreversible after the first scan.

The bands for ν-OH and the OCO of (bi)carbonate were integrated to provide semi-quantitative information on their potential-dependence in CTAB-free electrolytes (Figures 2 and S10, blue traces). The δ_{HOH} band overlaps with the (bi)carbonate desorption band, making it difficult to integrate. Therefore, we will only consider the ν-OH band integration in this discussion. It is worth noting that the potential-dependences of the ν-OH and δ_{HOH} band exhibit similar trends. In the forward scan direction (from 0.2 to −1.0 V), the integrated band intensity of ν-OH starts to increase at −0.1 V before plateauing at −0.2 V; then the intensity increased sharply as the voltage was swept negative of −0.4 V (Figure 2a). Simultaneously, we observed a desorption band for (bi)carbonate, which grew for E < 0.2 V before plateauing for $E \leq -0.4$ V. The potential of zero charge (PZC) of polycrystalline Cu is around −0.73 V (SHE) at pH 5.7 with a Nernstian shift of ∼0.059 V per pH unit, placing the PZC near

https://dx.doi.org/10.1021/acs.jpclett.0c01334
J. Phys. Chem. Lett. 2020, 11, 5457−5463

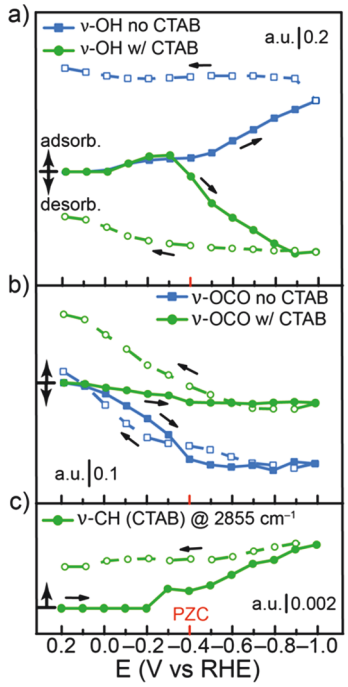

Figure 2. Integrated band intensities of the (a) ν-OH band, (b) ν-OCO band of (bi)carbonate and formate, (c) C−H bands of the CTAB headgroup collected during a cyclic voltammogram with a sweep rate of 10 mV s^{-1} starting from 0.2 to −1.0 V in the forward direction (solid lines) and −1.0 to 0.2 V in the reverse direction (dashed lines) in CO_2-saturated 0.1 M $NaHCO_3$ electrolyte with (green trace) an without (blue traces) 67 μM CTAB. The background spectrum was collected at 0.2 V vs RHE the respective solutions. Black arrows are shown as guides to indicate the scan direction.

−0.4 V vs RHE at pH 6.8.[46] The surface of Cu is rendered negative for voltages more negative than the PZC. A sharp increase in the ν-OH band intensity and a plateau of the (bi)carbonate band intensity coincide with the PZC of Cu (Figure 2a,b). The integrated band of the ν-OH band was found to increase over the course of 10 min (Figure S11). In the reverse scan direction (from −1.0 to 0.2 V) collected in the CTAB-free electrolyte, the ν-OH band maintained a positive intensity relative to the reference spectra across the entire voltage range, indicating irreversible adsorption of interfacial water (Figures 2a and S12a). This behavior is similar to what was observed in other reports.[36] The OCO band was found to exhibit reversible behavior as the reverse and forward traces nearly overlapped (Figures 2b and S12b). Similar behavior for the ν-OH and ν-OCO profiles were observed in NaBr-containing electrolytes (Figure S13). Taken together, the increase of the ν-OH band intensity and bleach of the (bi)carbonate band indicated that the orientation of water changed with potential, and its adsorption occurs with the desorption of (bi)carbonate.

To identify the role of CTAB, the integrated band intensities for the C−H band of CTAB's headgroup, ν-OH, and OCO were measured in CTAB-containing electrolyte (Figures 2 and S10, green traces). The forward scan direction shows that the absorption bands of CTAB's headgroup mirror the desorption bands for ν-OH for $E < -0.3$ V (Figure 2a,c). The integrated band intensity of the ν-OH band was stable over the course of 10 min (Figure S11). We also observed a desorption band for (bi)carbonate, which increases for $E < 0.2$ V before plateauing for $E \leq -0.4$ V, similar to what we observed for the CTAB-free electrolyte. The presence of CTAB displaces some of the (bi)carbonate at the reference voltage as shown by the difference in (bi)carbonate band intensity when the reference spectrum was changed from the CTAB-containing solution to a reference spectrum that does not contain CTAB (Figure S14). In the reverse scan direction (Figure 2c), the C−H band for CTAB's headgroup maintained a positive intensity, which barely decreased across the entire voltage range, suggesting that the head down organization and interfacial concentration of CTAB was maintained. In the reverse scan, the ν-OH desorption band maintained its negative intensity until the PZC; for $E >$ PZC, the desorption band intensity decreased. The OCO band was found to increase to positive adsorption values for $E >$ PZC in the reverse scan; however, this band is convoluted by the presence of the OCO band of interfacial formate that was produced from the CO_2RR (Figure S12d). Taken together, this data indicated that the accumulation and reorientation of CTAB at the interface was irreversible when the electrode was cathodically polarized, and that its presence was responsible for disrupting water's hydrogen-bonding network, causing the desorption of water from the interface. We hypothesize that interfacial water is the primary proton source for HER; if this is true, then the rate of j_{H2} should correlate with the intensity of the ν-OH desorption band.

To gain further insight on the role of CTAB in suppressing HER and CO_2RR, we evaluated the ν-OH band as a function of CTAB concentration at −0.8 V with the reference spectrum collected in a CTAB-free electrolyte at −0.8 V (Figure 3a).

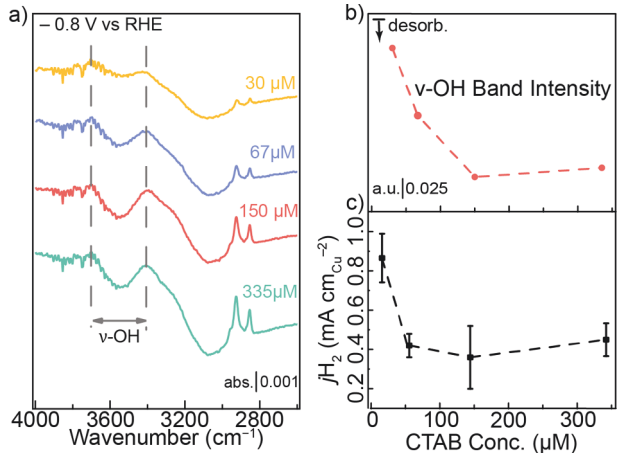

Figure 3. (a) Representative infrared spectra of the water ν-OH band for various CTAB concentrations. (b) Integrated band intensity and (c) ECSA normalized current density for HER as a function of CTAB concentration. Dashed lines serve only as a guide to connect the data points together. All data was collected in CO_2-saturated 0.1 M $NaHCO_3$ electrolyte at −0.8 V vs RHE with CTAB concentrations of 30, 67, 150, and 335 μM. All spectra were backgrounded to the CTAB-free electrolyte at −0.8 V vs RHE.

The intensity of ν-OH desorption grew as the concentration of CTAB was increased from 30 to 150 μM and then slightly decreased at 335 μM CTAB. The slight decrease in the integrated band intensity at 335 μM is probably from the formation of CTAB micelles, which are known to exhibit decreased critical micelle concentration (CMC) in electrolyte solutions relative to pure water; additionally, the interfacial CTAB concentration may be higher than the bulk solution concentration.[47] The j_{H2} was measured as a function of CTAB

https://dx.doi.org/10.1021/acs.jpclett.0c01334
J. Phys. Chem. Lett. 2020, 11, 5457−5463

concentration and compared with the ν-OH integrated band intensity at −0.8 V (Figure 3a,b). The j_{H2} was systematically attenuated by >2× as the concentration of CTAB increased from 30 to 150 μM, then slightly increased at 335 μM CTAB (Figure 3c). The intensity of ν-OH desorption band mirrors $j_{H2,}$ indicating that interfacial water is a facile proton donor for HER and CO_2RR. This notion is supported by various reports that indicate that H_2O is the source of protons for CO_2RR and HER.[28,29] Solution based proton donors, such as H_2O or HCO_3^-, have not been invoked to be part of the rate-limiting step for CO or $HCOO^-$ production during CO_2RR; therefore, a reduction in interfacial proton donor concentration would not suppress the formation of these products.[9,10,48] In contrast, protons are part of the rate-limiting step for HER; hence, a reduction in the interfacial proton donor concentration will suppress this reaction.[9,10]

To understand the enhancement in CO_2RR selectivity and activity in CTAB-containing electrolytes, the potential-dependence of the CO bands was investigated. Atop-CO (CO bound to a single atom) was observed at frequencies > 1900 cm^{-1}, while bridge-bonded CO (CO bound to ≥2 atoms) was observed in the range of 1800 to 1900 cm^{-1} (Figure 1b,d).[36,37,49] Bridge-bonded CO is a kinetically incompetent species for CO_2RR on Cu electrodes; hence, it will not be considered in this discussion.[16] We observe two atop-CO bands at 2096 cm^{-1} (atop-CO bound to step sites) and 2055 cm^{-1} (atop-CO bound to terrace sites) in CTAB-free electrolytes, which appear at −0.1 and −0.3 V, respectively.[49,50] An additional band at ∼1998 cm^{-1} appears after CTAB addition, suggesting that the local Cu-bound CO environment is distinct from CTAB-free conditions. Notably, the frequency of all of the atop-CO adsorption bands shifts with potential, indicating that these species are specifically adsorbed onto the Cu surface.[51] The low frequency atop-CO band probably arises from an enhanced interfacial electrostatic field via the ligand effect of coadsorbed CTAB with CO.[23,49,52−54] The low frequency of this new atop-CO band indicated this CO species is more activated, as evidenced by a weaker C−O bond stretching frequency compared to the frequency of atop-CO species without CTAB. The integrated band intensity of all the atop-CO bands in CTAB-free electrolyte slowly rises in intensity from 0.1 to −0.7 V, before increasing rapidly for E < −0.7 V (Figure 4a). In contrast, the atop-CO in CTAB-containing electrolyte appeared at −0.2 V but hardly changed in intensity until −0.6 V, the nit rapidly grew in intensity (Figure 4a). The rapid increase of the integrated band intensity for atop-CO coincided with the increased rate of j_{CO} (Figure 4b). We tracked the integrated band intensity for the atop-CO as a function of time at −0.8 V,and we found the integrated band intensity decreased by ∼20 and 50% for CTAB-free and CTAB electrolytes, respectively, before stabilizing after ∼400 s (Figure S15). Although the integrated band intensity of the atop-CO bands also tracked similarly with j_{HCOO-}, we are hesitant to associate it to formate production, since other studies have indicated that it forms through an O-bound *COOH intermediate or via direct hydrogenation of CO_2 with H*.[55,56] Surface adsorbed *COOH intermediates on Cu are usually observed near ∼1380 cm^{-1}; however, multiple C−H vibrational bands from CTAB appeared between ∼1320−1500 cm^{-1}, obscuring the observation of bound intermediates responsible for formate production.[57] Taken together, this data indicates that a larger population of atop-CO and the appearance of the low frequency CO band can be correlated with enhanced CO production.

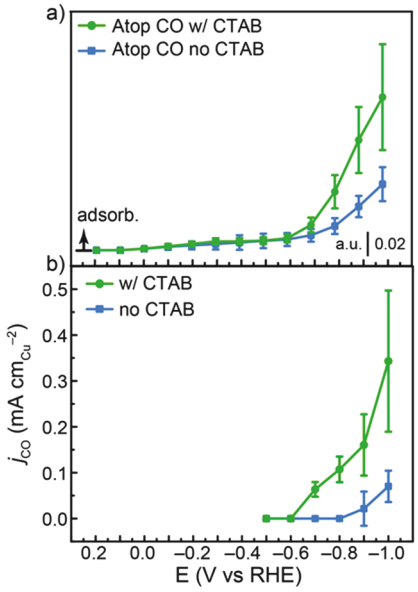

Figure 4. (a) Integrated band intensity of atop-CO collected during a linear sweep voltammogram at a 10 mV s^{-1} scan rate and (b) partial current density for CO formation collected by constant potential electrolysis in CO_2-saturated 0.1 M $NaHCO_3$ electrolyte with and without 67 μM CTAB. The background spectrum was collected at 0.2 V vs RHE in the respective solutions.

In conclusion, we used SEIRAS to investigate dynamics of interfacial water, CO intermediates, and a molecular promotor (CTAB) on Cu electrodes under CO_2 reduction conditions. Our results suggest that the promotion of CO_2 reduction by CTAB is from a combination of HER suppression and the enhancement of the CO_2RR rate. The ν-OH band has been used to describe the reorganization of water at the interface from the presence of adsorbed CTAB. The bleach of the ν-OH and δ_{H2O} bands indicated that the concentration of interfacial water is reduced. The fact that CTAB is adsorbed at the interface and that its irreversible reorientation and accumulation can be correlated to removal of water from the double layer gives credence to the unproven assumption that the assembly of the surfactant controls the supply of water, the principle proton donor, to the electrode interface. The removal of interfacial water is most likely driven by steric and hydrophobic effects from the alkane chain of CTAB. The decreased rate of HER was shown to systematically correlate with the increased intensity of the water desorption band, verifying that interfacial water is a facile proton donor under CO_2RR conditions. The presence of CTAB near the electrode surface perturbs the binding configuration of CO as evidenced by the observation of a low frequency atop-CO band. In addition, the higher CO surface coverage and the more activated CO molecule plays a critical role in enhancing the rate of CO formation. This study demonstrates that modification of the electric double layer with a cationic surfactant is a powerful method for enhancing CO_2RR reduction activity while simultaneously inhibiting the rate for HER.

https://dx.doi.org/10.1021/acs.jpclett.0c01334
J. Phys. Chem. Lett. 2020, 11, 5457−5463

■ ASSOCIATED CONTENT

Supporting Information

The Supporting Information is available free of charge at https://pubs.acs.org/doi/10.1021/acs.jpclett.0c01334.

Experimental methods and Figures S1−S15 as described in the text (PDF)

■ AUTHOR INFORMATION

Corresponding Author

Anthony Shoji Hall − *Department of Materials Science and Engineering and Department of Chemistry, Johns Hopkins University, Baltimore, Maryland 21218, United States;* orcid.org/0000-0003-4134-4160; Email: shoji@jhu.edu

Authors

Zhuo-Qun Zhang − *Department of Materials Science and Engineering, Johns Hopkins University, Baltimore, Maryland 21218, United States*

Soumyodip Banerjee − *Department of Chemistry, Johns Hopkins University, Baltimore, Maryland 21218, United States*

V. Sara Thoi − *Department of Materials Science and Engineering and Department of Chemistry, Johns Hopkins University, Baltimore, Maryland 21218, United States;* orcid.org/0000-0003-0896-4077

Complete contact information is available at: https://pubs.acs.org/10.1021/acs.jpclett.0c01334

Notes

The authors declare no competing financial interest.

■ ACKNOWLEDGMENTS

A.S.H. acknowledges financial support from the National Science Foundation under award no. CHE-1764310. We also acknowledge the assistance of Dr. Marina A. Solomos and Prof. Thomas Kempa for their assistance in metal evaporation. V.S.T. and S.B. also thank the Department of Chemistry and Johns Hopkins University for instrumentation support, graduate student support, and start-up funding. We also thank Prof. Marcel Schreier and Prof. Chris Hendon for helpful discussion.

■ REFERENCES

(1) Mariano, R. G.; McKelvey, K.; White, H. S.; Kanan, M. W. Selective increase in CO_2 electroreduction activity at grain-boundary surface terminations. *Science* **2017**, *358* (6367), 1187−1192.

(2) Kramer, W. W.; McCrory, C. C. L. Polymer coordination promotes selective CO2 reduction by cobalt phthalocyanine. *Chemical Science* **2016**, *7* (4), 2506−2515.

(3) Hahn, C.; Hatsukade, T.; Kim, Y.-G.; Vailionis, A.; Baricuatro, J. H.; Higgins, D. C.; Nitopi, S. A.; Soriaga, M. P.; Jaramillo, T. F. Engineering Cu surfaces for the electrocatalytic conversion of CO_2: Controlling selectivity toward oxygenates and hydrocarbons. *Proc. Natl. Acad. Sci. U. S. A.* **2017**, *114* (23), 5918−5923.

(4) Wang, L.; Nitopi, S.; Wong, A. B.; Snider, J. L.; Nielander, A. C.; Morales-Guio, C. G.; Orazov, M.; Higgins, D. C.; Hahn, C.; Jaramillo, T. F. Electrochemically converting carbon monoxide to liquid fuels by directing selectivity with electrode surface area. *Nature Catalysis* **2019**, *2* (8), 702−708.

(5) Dinh, C.-T.; Burdyny, T.; Kibria, M. G.; Seifitokaldani, A.; Gabardo, C. M.; García de Arquer, F. P.; Kiani, A.; Edwards, J. P.; De Luna, P.; Bushuyev, O. S.; Zou, C.; Quintero-Bermudez, R.; Pang, Y.; Sinton, D.; Sargent, E. H. CO_2 electroreduction to ethylene via hydroxide-mediated copper catalysis at an abrupt interface. *Science* **2018**, *360* (6390), 783−787.

(6) Hori, Y.; Takahashi, I.; Koga, O.; Hoshi, N. Selective Formation of C2 Compounds from Electrochemical Reduction of CO2 at a Series of Copper Single Crystal Electrodes. *J. Phys. Chem. B* **2002**, *106* (1), 15−17.

(7) Garza, A. J.; Bell, A. T.; Head-Gordon, M. Mechanism of CO2 Reduction at Copper Surfaces: Pathways to C2 Products. *ACS Catal.* **2018**, *8* (2), 1490−1499.

(8) Nie, X.; Esopi, M. R.; Janik, M. J.; Asthagiri, A. Selectivity of CO2 Reduction on Copper Electrodes: The Role of the Kinetics of Elementary Steps. *Angew. Chem., Int. Ed.* **2013**, *52* (9), 2459−2462.

(9) Hall, A. S.; Yoon, Y.; Wuttig, A.; Surendranath, Y. Mesostructure-Induced Selectivity in CO2 Reduction Catalysis. *J. Am. Chem. Soc.* **2015**, *137* (47), 14834−14837.

(10) Yoon, Y.; Hall, A. S.; Surendranath, Y. Tuning of Silver Catalyst Mesostructure Promotes Selective Carbon Dioxide Conversion into Fuels. *Angew. Chem., Int. Ed.* **2016**, *55* (49), 15282−15286.

(11) Thorson, M. R.; Siil, K. I.; Kenis, P. J. A. Effect of Cations on the Electrochemical Conversion of CO2 to CO. *J. Electrochem. Soc.* **2013**, *160* (1), F69−F74.

(12) Singh, M. R.; Kwon, Y.; Lum, Y.; Ager, J. W.; Bell, A. T. Hydrolysis of Electrolyte Cations Enhances the Electrochemical Reduction of CO2 over Ag and Cu. *J. Am. Chem. Soc.* **2016**, *138* (39), 13006−13012.

(13) Banerjee, S.; Han, X.; Thoi, V. S. Modulating the Electrode−Electrolyte Interface with Cationic Surfactants in Carbon Dioxide Reduction. *ACS Catal.* **2019**, *9* (6), 5631−5637.

(14) Resasco, J.; Chen, L. D.; Clark, E.; Tsai, C.; Hahn, C.; Jaramillo, T. F.; Chan, K.; Bell, A. T. Promoter Effects of Alkali Metal Cations on the Electrochemical Reduction of Carbon Dioxide. *J. Am. Chem. Soc.* **2017**, *139* (32), 11277−11287.

(15) Trindell, J. A.; Clausmeyer, J.; Crooks, R. M. Size Stability and H2/CO Selectivity for Au Nanoparticles during Electrocatalytic CO2 Reduction. *J. Am. Chem. Soc.* **2017**, *139* (45), 16161−16167.

(16) Gunathunge, C. M.; Ovalle, V. J.; Li, Y.; Janik, M. J.; Waegele, M. M. Existence of an Electrochemically Inert CO Population on Cu Electrodes in Alkaline pH. *ACS Catal.* **2018**, *8* (8), 7507−7516.

(17) Han, Z.; Kortlever, R.; Chen, H.-Y.; Peters, J. C.; Agapie, T. CO2 Reduction Selective for C ≥ 2 Products on Polycrystalline Copper with N-Substituted Pyridinium Additives. *ACS Cent. Sci.* **2017**, *3* (8), 853−859.

(18) Cao, Z.; Kim, D.; Hong, D.; Yu, Y.; Xu, J.; Lin, S.; Wen, X.; Nichols, E. M.; Jeong, K.; Reimer, J. A.; Yang, P.; Chang, C. J. A Molecular Surface Functionalization Approach to Tuning Nanoparticle Electrocatalysts for Carbon Dioxide Reduction. *J. Am. Chem. Soc.* **2016**, *138* (26), 8120−8125.

(19) Rosen, B. A.; Salehi-Khojin, A.; Thorson, M. R.; Zhu, W.; Whipple, D. T.; Kenis, P. J. A.; Masel, R. I. Ionic Liquid−Mediated Selective Conversion of CO_2 to CO at Low Overpotentials. *Science* **2011**, *334* (6056), 643−644.

(20) Lau, G. P. S.; Schreier, M.; Vasilyev, D.; Scopelliti, R.; Grätzel, M.; Dyson, P. J. New Insights Into the Role of Imidazolium-Based Promoters for the Electroreduction of CO2 on a Silver Electrode. *J. Am. Chem. Soc.* **2016**, *138* (25), 7820−7823.

(21) Dunwell, M.; Yan, Y.; Xu, B. In Situ Infrared Spectroscopic Investigations of Pyridine-Mediated CO2 Reduction on Pt Electrocatalysts. *ACS Catal.* **2017**, *7* (8), 5410−5419.

(22) Ovalle, V. J.; Waegele, M. M. Understanding the Impact of N-Arylpyridinium Ions on the Selectivity of CO2 Reduction at the Cu/Electrolyte Interface. *J. Phys. Chem. C* **2019**, *123* (40), 24453−24460.

(23) Sarkar, S.; Maitra, A.; Banerjee, S.; Thoi, V. S.; Dawlaty, J. M. Electric Fields at Metal−Surfactant Interfaces: A Combined Vibrational Spectroscopy and Capacitance Study. *J. Phys. Chem. B* **2020**, *124* (7), 1311−1321.

(24) Quan, F.; Xiong, M.; Jia, F.; Zhang, L. Efficient electroreduction of CO2 on bulk silver electrode in aqueous solution via the inhibition of hydrogen evolution. *Appl. Surf. Sci.* **2017**, *399*, 48−54.

(25) Li, J.; Li, X.; Gunathunge, C. M.; Waegele, M. M. Hydrogen bonding steers the product selectivity of electrocatalytic CO reduction. *Proc. Natl. Acad. Sci. U. S. A.* **2019**, *116* (19), 9220−9229.

(26) Dong, Q.; Zhang, X.; He, D.; Lang, C.; Wang, D. Role of H2O in CO2 Electrochemical Reduction As Studied in a Water-in-Salt System. *ACS Cent. Sci.* **2019**, *5* (8), 1461−1467.
(27) Han, X.; Wang, M.; Le, M. L.; Bedford, N. M.; Woehl, T. J.; Thoi, V. S. Effects of substrate porosity in carbon aerogel supported copper for electrocatalytic carbon dioxide reduction. *Electrochim. Acta* **2019**, *297*, 545−552.
(28) Goyal, A.; Marcandalli, G.; Mints, V. A.; Koper, M. T. M. Competition between CO2 Reduction and Hydrogen Evolution on a Gold Electrode under Well-Defined Mass Transport Conditions. *J. Am. Chem. Soc.* **2020**, *142* (9), 4154−4161.
(29) Ooka, H.; Figueiredo, M. C.; Koper, M. T. M. Competition between Hydrogen Evolution and Carbon Dioxide Reduction on Copper Electrodes in Mildly Acidic Media. *Langmuir* **2017**, *33* (37), 9307−9313.
(30) Buckley, A. K.; Lee, M.; Cheng, T.; Kazantsev, R. V.; Larson, D. M.; Goddard, W. A., Iii; Toste, F. D.; Toma, F. M. Electrocatalysis at Organic−Metal Interfaces: Identification of Structure−Reactivity Relationships for CO2 Reduction at Modified Cu Surfaces. *J. Am. Chem. Soc.* **2019**, *141* (18), 7355−7364.
(31) Bao, W.-J.; Yan, Z.-D.; Wang, M.; Zhao, Y.; Li, J.; Wang, K.; Xia, X.-H.; Wang, Z.-L. Distance-determined sensitivity in attenuated total reflection-surface enhanced infrared absorption spectroscopy: aptamer−antigen compared to antibody−antigen. *Chem. Commun.* **2014**, *50* (58), 7787−7789.
(32) Osawa, M. Chapter 7 - Electrocatalytic Reactions on Platinum Electrodes Studied by Dynamic Surface-Enhanced Infrared Absorption Spectroscopy (SEIRAS). *In-situ Spectroscopic Studies of Adsorption at the Electrode and Electrocatalysis* **2007**, 209−246.
(33) Osawa, M. Surface-Enhanced Infrared Absorption. *Near-Field Optics and Surface Plasmon Polaritons* **2001**, *81*, 163−187.
(34) Wuttig, A.; Surendranath, Y. Impurity Ion Complexation Enhances Carbon Dioxide Reduction Catalysis. *ACS Catal.* **2015**, *5* (7), 4479−4484.
(35) Leung, K. Y.; McCrory, C. C. L. Effect and Prevention of Trace Ag+ Contamination from Ag/AgCl Reference Electrodes on CO2 Reduction Product Distributions at Polycrystalline Copper Electrodes. *ACS Applied Energy Materials* **2019**, *2* (11), 8283−8293.
(36) Wuttig, A.; Liu, C.; Peng, Q.; Yaguchi, M.; Hendon, C. H.; Motobayashi, K.; Ye, S.; Osawa, M.; Surendranath, Y. Tracking a Common Surface-Bound Intermediate during CO2-to-Fuels Catalysis. *ACS Cent. Sci.* **2016**, *2* (8), 522−528.
(37) Heyes, J.; Dunwell, M.; Xu, B. CO2 Reduction on Cu at Low Overpotentials with Surface-Enhanced in Situ Spectroscopy. *J. Phys. Chem. C* **2016**, *120* (31), 17334−17341.
(38) Osawa, M.; Tsushima, M.; Mogami, H.; Samjeské, G.; Yamakata, A. Structure of Water at the Electrified Platinum−Water Interface: A Study by Surface-Enhanced Infrared Absorption Spectroscopy. *J. Phys. Chem. C* **2008**, *112* (11), 4248−4256.
(39) Ataka, K.-i.; Yotsuyanagi, T.; Osawa, M. Potential-Dependent Reorientation of Water Molecules at an Electrode/Electrolyte Interface Studied by Surface-Enhanced Infrared Absorption Spectroscopy. *J. Phys. Chem.* **1996**, *100* (25), 10664−10672.
(40) Zhu, S.; Li, T.; Cai, W.-B.; Shao, M. CO2 Electrochemical Reduction As Probed through Infrared Spectroscopy. *ACS Energy Letters* **2019**, *4* (3), 682−689.
(41) Yang, K.; Kas, R.; Smith, W. A. In Situ Infrared Spectroscopy Reveals Persistent Alkalinity near Electrode Surfaces during CO2 Electroreduction. *J. Am. Chem. Soc.* **2019**, *141* (40), 15891−15900.
(42) Sovago, M.; Campen, R. K.; Wurpel, G. W. H.; Müller, M.; Bakker, H. J.; Bonn, M. Vibrational Response of Hydrogen-Bonded Interfacial Water is Dominated by Intramolecular Coupling. *Phys. Rev. Lett.* **2008**, *100* (17), 173901.
(43) Wuttig, A.; Ryu, J.; Surendranath, Y. Electrolyte Competition Controls Surface Binding of CO Intermediates to CO2 Reduction Catalysts. *chemRxiv* **2019**.
(44) Kung, K. H. S.; Hayes, K. F. Fourier transform infrared spectroscopic study of the adsorption of cetyltrimethylammonium bromide and cetylpyridinium chloride on silica. *Langmuir* **1993**, *9* (1), 263−267.
(45) Viana, R. B.; da Silva, A. B. F.; Pimentel, A. S. Infrared Spectroscopy of Anionic, Cationic, and Zwitterionic Surfactants. *Adv. Phys. Chem.* **2012**, *2012*, 903272.
(46) Łukomska, A.; Sobkowski, J. Potential of zero charge of monocrystalline copper electrodes in perchlorate solutions. *J. Electroanal. Chem.* **2004**, *567* (1), 95−102.
(47) Kumar, B.; Tikariha, D.; Ghosh, K. K. Effects of Electrolytes on Micellar and Surface Properties of Some Monomeric Surfactants. *J. Dispersion Sci. Technol.* **2012**, *33* (2), 265−271.
(48) Wuttig, A.; Yoon, Y.; Ryu, J.; Surendranath, Y. Bicarbonate Is Not a General Acid in Au-Catalyzed CO2 Electroreduction. *J. Am. Chem. Soc.* **2017**, *139* (47), 17109−17113.
(49) Hollins, P. The influence of surface defects on the infrared spectra of adsorbed species. *Surf. Sci. Rep.* **1992**, *16* (2), 51−94.
(50) Borguet, E.; Dai, H. L. Site-specific properties and dynamical dipole coupling of CO molecules adsorbed on a vicinal Cu(100) surface. *J. Chem. Phys.* **1994**, *101* (10), 9080−9095.
(51) Berná, A.; Rodes, A.; Feliu, J. M. Chapter 1 - In-situ FTIR Studies on the Acid−Base Equilibria of Adsorbed Species on Well-Defined Metal Electrode Surfaces. *In-situ Spectroscopic Studies of Adsorption at the Electrode and Electrocatalysis* **2007**, 1−32.
(52) Akhade, S. A.; McCrum, I. T.; Janik, M. J. The Impact of Specifically Adsorbed Ions on the Copper-Catalyzed Electroreduction of CO2. *J. Electrochem. Soc.* **2016**, *163* (6), F477−F484.
(53) Rodriguez, J. A.; Campbell, C. T. Quantum chemical studies of the effects of electron-transferring ligands upon carbon monoxide chemisorption on copper(100). *J. Phys. Chem.* **1987**, *91* (8), 2161−2171.
(54) McCrum, I. T.; Hickner, M. A.; Janik, M. J. Quaternary Ammonium Cation Specific Adsorption on Platinum Electrodes: A Combined Experimental and Density Functional Theory Study. *J. Electrochem. Soc.* **2018**, *165* (2), F114−F121.
(55) Cheng, T.; Xiao, H.; Goddard, W. A. Reaction Mechanisms for the Electrochemical Reduction of CO2 to CO and Formate on the Cu(100) Surface at 298 K from Quantum Mechanics Free Energy Calculations with Explicit Water. *J. Am. Chem. Soc.* **2016**, *138* (42), 13802−13805.
(56) Katayama, Y.; Nattino, F.; Giordano, L.; Hwang, J.; Rao, R. R.; Andreussi, O.; Marzari, N.; Shao-Horn, Y. An In Situ Surface-Enhanced Infrared Absorption Spectroscopy Study of Electrochemical CO2 Reduction: Selectivity Dependence on Surface C-Bound and O-Bound Reaction Intermediates. *J. Phys. Chem. C* **2019**, *123* (10), 5951−5963.
(57) Zhu, S.; Jiang, B.; Cai, W.-B.; Shao, M. Direct Observation on Reaction Intermediates and the Role of Bicarbonate Anions in CO2 Electrochemical Reduction Reaction on Cu Surfaces. *J. Am. Chem. Soc.* **2017**, *139* (44), 15664−15667.

https://dx.doi.org/10.1021/acs.jpclett.0c01334
J. Phys. Chem. Lett. 2020, 11, 5457−5463